*crystals*

*Article*

# Nucleation of L1$_2$-Al$_3$M (M = Sc, Er, Y, Zr) Nanophases in Aluminum Alloys: A First-Principles ThermodynamicsStudy

**Shuai Liu [1], Fangjun Liu [2], Zhanhao Yan [1], Baohua Nie [1,*], Touwen Fan [3], Dongchu Chen [1] and Yu Song [4,*]**

1 School of Materials Science and Hydrogen Energy, Foshan University, Foshan 528000, China; 2112206013@stu.fosu.edu.cn (S.L.); 20210580109@stu.fosu.edu.cn (Z.Y.); chendc@fosu.edu.cn (D.C.)
2 School of Mechatronic Engineering and Automation, Foshan University, Foshan 528000, China; liufj@fosu.edu.cn
3 Research Institute of Automobile Parts Technology, Hunan Institute of Technology, Hengyang 421002, China; 2021001018@hnit.edu.cn
4 Shenzhen Rspower Technology Co., Ltd., Shenzhen 518000, China
* Correspondence: niebaohua@fosu.edu.cn (B.N.); songyu188200@foxmail.com (Y.S.); Tel.: +86-075782700525 (B.N.); +86-75583233458 (Y.S.)

**Abstract:** High-performance Sc-containing aluminum alloys are limited in their industrial application due to the high cost of Sc elements. Er, Zr, and Y elements are candidates for replacing Sc elements. Combined with the first-principles thermodynamic calculation and the classical nucleation theory, the nucleation of L1$_2$-Al$_3$M (M = Sc, Er, Y, Zr) nanophases in dilutealuminum alloys were investigated to reveal their structural stability. The calculated results showed that the critical radius and nucleation energy of the L1$_2$-Al$_3$M phases were as follows: Al$_3$Er > Al$_3$Y > Al$_3$Sc > Al$_3$Zr. The Al$_3$Zr phase was the easiest to nucleate in thermodynamics, while the nucleation of the Al$_3$Y and Al$_3$Er phases were relatively difficult in thermodynamics. Various structures of Al$_3$(Y, Zr) phases with the radius r < 1 nm can coexist in Al-Y-Zr alloys. At a precipitate's radius of 1–10 nanometers, the core–shelled Al$_3$Zr(Y) phase illustrated the highest nucleation energy, while the separated structure Al$_3$Zr/Al$_3$Y obtained the lowest one, and had thermodynamic advantages in the nucleation process. Moreover, the core–shelled Al$_3$Zr(Y) phase obtained a higher nucleation energy than Al$_3$Zr(Sc) and Al$_3$Zr(Er). Core–doubleshelled Al$_3$Zr/Er(Y) obtained a lower nucleation energy than that of Al$_3$Zr(Y) due to the negative $\Delta G_{chem}$ of Al$_3$Er and the negative Al$_3$Er/Al$_3$Y interfacial energy, and was preferentially precipitated in thermodynamics stability.

**Keywords:** Al$_3$Y; nucleation; first-principles; aluminum alloy

check for updates

**Citation:** Liu, S.; Liu, F.; Yan, Z.; Nie, B.; Fan, T.; Chen, D.; Song, Y. Nucleation of L1$_2$-Al$_3$M (M = Sc, Er, Y, Zr) Nanophases in Aluminum Alloys: A First-Principles ThermodynamicsStudy. *Crystals* **2023**, *13*, 1228. https://doi.org/10.3390/cryst13081228

Academic Editor: Wangzhong Mu

Received: 14 July 2023
Revised: 2 August 2023
Accepted: 7 August 2023
Published: 9 August 2023



## 1. Introduction

Sc-containing aluminum alloys are ideal materials for key components in the aerospace, high-speed rail, and automobile industries due to their high strength, corrosion resistance, and formability [1–3]. L1$_2$-Al$_3$Sc nanoparticles precipitated in Sc-containing aluminum alloys can effectively inhibit the recrystallization process [4], thereby obtaining comprehensive properties such as high strength, toughness, and corrosion resistance. Moreover, Seidman et al. [5,6] developed a series of Al-Sc high-temperature aluminum alloys. However, due to the high diffusion rate of Sc atoms, L1$_2$-Al$_3$Sc nanoparticles are prone to coarsening, reducing their ability to inhibit recrystallization and high-temperature performance. On the other hand, Zr atoms can partially replace Sc atoms in the Al$_3$Sc nanophase, forming a core–shelled Al$_3$(Sc$_{1-x}$, Zr$_x$), namely an Al$_3$Sc core and Al$_3$Zr shell) [7], where the Al$_3$Zr shell improves the coarsening resistance of the Al$_3$(Sc$_{1-x}$, Zr$_x$) nanophase due to the low diffusion rate of Zr atoms in the aluminum matrix [8].

However, the high cost of Sc elements greatly limits the engineering application of Sc-containing aluminum alloys. As members of the Sc element family, Er, Yb rare earth elements and the Y element have been considered ideal substitutes for Sc elements. Er and Yb elements were reported to form a core–shell structure of $Al_3$(Er, Zr) [9,10] and $Al_3$(Yb, Zr) [11,12] nanophases, which also effectively inhibited the recrystallization of aluminum alloys. Based on high-throughput first-principles calculations of the nucleation and growth for the $L1_2$structure $Al_3$RE phases, Fan et al. [13,14] revealed the $\Delta G_V$ firstly decreased from Sc, Y to Ce, then increased linearly for RE elements, and the $\Delta G_V$ tended to increase linearly with the temperature. It was speculated that the Y element could replace the expensive Sc element.The investigation by Zhang et al. [15,16] showed that the precipitation phase was mainly the $Al_3$Y phase, which became the core of $Al_3$Zr and promoted the precipitation kinetics of solid solution Zr atoms, whereas a hybrid structure of $Al_3$(Zr, Y) rather than the typical core–shelled structure was observed after long-term homogenization, where the Y and Zr elements were uniformly distributed in $Al_3$(Y, Zr) nanoprecipitates through atom probe tomography (APT).

Some research has been conducted on the formation mechanism of the hybrid structure of $Al_3$(Zr, Y). Zhang et al. [16] indicated that the hybrid structure of $Al_3$(Zr, Y) was attributed to the strong interactions between the Y and Zr atoms, resulting in their co-precipitation. Based on first-principles calculations, Wang et al. [17] indicated that the doping of the Y element and the Zr element decreased the interface energies of the FCC-Al(001)/FCC-$Al_3$Y(001) interface and formed a hybrid structure of $Al_3$(Y, Zr) instead of an $Al_3$Y core + $Al_3$Zr shell structure. The author's previous research indicated that the interface energy of $Al_3$Zr/Al was lower than that of $Al_3$Zr/$Al_3$Y, and it was deduced that $Al_3$Zr tended to form a shell layer, while $Al_3$Y formed a core layer. However, the high coherent strain energy made the $Al_3$Y/$Al_3$Zr interface unstable, and it was difficult to form a stable cored $Al_3$Y/shelled $Al_3$Zr structure [18]. Although the author's previous investigation elucidated the reason for $Al_3$Y/$Al_3$Zr not having a core–shelled structure based on the coherent strain energy, there were several issues that needed to be answered, such as whether the hybrid structure of $Al_3$(Zr, Y) was determined by atomic diffusion control or thermodynamic structure stability.

One view was that the formation of the core–shelled $Al_3$M phase was attributed to the differences in atomic diffusion rates. $Al_3$Sc and $Al_3$Er core structures were formed due to the fast diffusion rate of the Sc and Er atoms. The diffusion rate of the Zr element was slow, resulting in the formation of an $Al_3$Zr shell structure [19]. Furthermore, the core($Al_3$Er)–double shell ($Al_3$Sc/$Al_3$Zr) structure of $L1_2$-$Al_3$(Sc, Er, Zr) was precipitated in Al-Sc-Er-Zr alloys after homogenization at 400 °C [20]. Seidman et al. [20] suggested that the core–double-shelled $L1_2$-$Al_3$(Sc, Er, Zr) can be attributed to their difference in diffusion rate, e.g., $D_{Er} > D_{Sc} > D_{Zr}$. Leibner et al. [21] found that there were two major groups of core–double-shelled $L1_2$-$Al_3$(Sc, Er, Zr) observed after aging at 600 °C/4 h, one having the usual core ($Al_3$Er)–double shell ($Al_3$Sc/$Al_3$Zr) structure and the other having an unusual core ($Al_3$Sc)–double shell ($Al_3$Er/$Al_3$Zr) structure. They suggested that the segregation of the Sc atom to dislocations and the interaction between the solid solution atoms and the Sc atom promoted the formation of the unusual core ($Al_3$Sc)–double shell structure. It should be noted that the hybrid structure of $Al_3$(Zr, Sc) [22] and $Al_3$(Er, Zr) [23] was also observed in aluminum alloys. Therefore, the difference in diffusion rates between atoms does not explain the formation of core–shelled structures well.

The thermodynamic analysis of nanophases' nucleation based on first-principles calculations can provide insights into the phase transformation process of $L1_2$-$Al_3$M phases. Jiang et al. [24,25] used first-principles calculation methods to calculate the nucleation energies of the $Al_3$(Er, Zr) and $Al_3$(Sc, Zr) phases with different microstructures, revealing the thermodynamic stability of the $Al_3$(Er, Zr) and $Al_3$(Sc, Zr) phases during the homogenization precipitation. The nucleation properties calculated by Liu [26] showed that the core–shelled $Al_3$(Er1−x, Scx) obtained a highly stable structure due to its low nucleation energy, which was independent of the temperature and Sc/Er ratio. However, first-principles calculations of the nucleation and thermodynamic stability for the $Al_3$(Y, Zr) phase were rarely reported. Furthermore, the author's investigation showed that Er atoms tended to segregate at the $Al_3$Y/$Al_3$Zr interface, and were inclined to form a core–double-shelled

$Al_3$(Y, Er, Zr) structure with an $Al_3Y$ core, an $Al_3Er$ inner shell, and an $Al_3Zr$ outer shell [18]. The nucleation and thermodynamic stability of core–double-shelled $Al_3$(Y, Er, Zr) needed to be evaluated to develop Al-Y-Zr series alloys.

Combining with the calculation results of interface energies and the coherent strain energy in the previous research [18], the total nucleation energies of various structures of $L1_2$-$Al_3M$ (M = Sc, Er, Zr, Y)phases were calculated based on first-principles thermodynamic calculation and classical nucleation theory. The critical nucleation energies and nucleation radii of $Al_3M$ phases were calculated to compare the nucleation differences of $Al_3M$ nanophases. The nucleation energies of various structures of ternary $L1_2$-$Al_3$(Y, Zr) phases were investigated to reveal the formation mechanism of $Al_3$(Y, Zr) with a hybrid structure. The nucleation calculation result of core–shelled $Al_3$(Y, Zr) was also compared with that of core–shelled $Al_3$(Sc, Zr) and core–shelled $Al_3$(Er, Zr). Furthermore, based on first-principles calculations, the nucleation energy of the core–double-shelled $Al_3$(Er, Y, Zr) phase was investigated to evaluate its thermodynamic stability. This paper aimed to reveal the internal formation mechanism of $L1_2$-$Al_3M$ with a core–shelled structure from the perspective of first-principles thermodynamic calculations, and provided guidance for the development of new Al-Y-Zr series alloys

## 2. Computational Methods

Based on density functional theory (DFT) [27], first-principles calculations were carried out by VASP software [28]. The electron configuration was described by Al-$3s^2 3p^1$, Sc-$3s^2 3p^6 4s^1 3d^2$, Zr-$4s^2 4p^6 5s^1 4d^3$, Er-$6s^2 5p^6 5d^1$, and Y-$4s^2 4p^6 5s^1 4d^2$ valence states, respectively. The ion–electron interactions were described by the projection augmented wave (PAW) method withinthe frozen core approximation [29]. The exchange-correlation energy functional between electrons was described by the Perdew–Burke–Ernzerhof (PBE) [30,31] method of generalized gradient approximation (GGA). The kinetic energy cutoff of the plane wave basis and the size of the k-mesh for the Brillouin zone were tested for self-consistent convergence. The calculation of the bulk phase of $L1_2$-$Al_3M$ (M = Sc, Er, Y, Zr) used conventional single cells. In each periodic direction of reciprocal space, the geometric structure was optimized by the Monkhorst–Pack k-point grids with linear k-mesh analytical values of less than $0.032\pi/\text{Å}$. Using the linear tetrahedron method with the Blöchl correction, the total energy was calculated when the total energy converged to $10^{-4}$ eV/atom. The lattice constants (a) and bulk modulus (B) were predicted as fcc-Al (a = 4.042 Å and B = 78.2 GPa), $L1_2$-$Al_3Sc$ (a = 4.103 Å and B = 86.4 GPa), $L1_2$-$Al_3Zr$ (a = 4.108 Å and B = 102.3 GPa), and $L1_2$-$Al_3Er$ (a = 4.232 Å and B = 78.5 GPa), respectively, which agreed well with Ref. [26].

Vibration entropy had a significant influence on the chemical formation energy $\Delta G_{chem}$ corresponding to the precipitation of the $L1_2$-$Al_3M$ phase from the fcc-$Al_nM$ solutionmatrix. The calculation of vibration entropy was based on the method of the density functional perturbation theory (DFPT) [32] under the simple harmonic approximation, and the phonon spectrum of $Al_3M$ was calculated by using the $2 \times 2 \times 2$ supercell model. The $Al_nM$ was adopted by the $2 \times 2 \times 2$ supercell Al matrix, and the M atom was doped and dissolved in the center. In this method, a small external disturbance was introduced, and the linear response of the system was calculated based on this disturbance. By calculating the response function, the perturbation expression of the vibration frequency can be derived, resulting in the vibration entropy difference of the $Al_3M$ phase.

## 3. Results and Discussion

### *3.1. Nucleation of Binary $L1_2$-$Al_3M$ Phases*

According to the classical nucleation theory, the nucleation work consisted of two parts: the energy released by the precipitated phase from the Al matrix, and the energy from the new interface between the precipitated phase and the matrix. The precipitated phase was usually assumed to be a sphere with uniform density distribution. When the

$L1_2$-$Al_3M$ nanophases are precipitated from the Al matrix, their precipitation radius $R$ and nucleation work $\Delta G$ can be expressed as:

$$\Delta G = \frac{4\pi}{3}R^3 \cdot \Delta G_V + 4\pi R^2 \cdot \gamma \quad (1)$$

where $\gamma$ is the interface energy per unit area after subtracting the coherent strain energy. The Al(001)/$Al_3M$(001)-contacting facet was the most energy-favored orientation [18,24,25], and the interface energy of Al(001)/$Al_3M$(001) was calculated to estimate the critical nucleation works and nucleation radius. $\Delta G_V$ is the volume-free energy per unit volume, which is defined as:

$$\Delta G_V = \Delta G_{chem} + G_s \quad (2)$$

where $\Delta G_{chem}$ is the chemical formation energy corresponding to the precipitation of the $L1_2$-$Al_3M$ phase in the matrix; $G_s$ is the coherent strain energy.

The chemical reaction equation of the $Al_3M$ nanophase precipitation can be written as: $Al_nM$ = $Al_3M$ + (n − 3)Al; so its chemical energy is expressed as [33]:

$$\begin{aligned} \Delta G_{chem} &= G_{Al_3M} + (n-3)\mu_{Al} - G_{Al_nM} \\ &= \left(\Delta H_{Al_3M} - \Delta H_{Al_nM}\right) - T\left(\Delta S_{Al_3M} - \Delta S_{Al_nM}\right) \end{aligned} \quad (3)$$

Here $\Delta H_{Al_3M}$ and $\Delta H_{Al_nM}$ are the formation enthalpies of $L1_2$-$Al_3M$ and fcc-$Al_nM$, respectively, and the enthalpy can be approximately equal to the internal energy here because the volume–pressure term in the solid state can be ignored [33]; $\Delta S_{Al_3M}$ and $\Delta S_{Al_nM}$ are the formation entropy of $L1_2$-$Al_3M$ and fcc-$Al_nM$, respectively.As the nucleation process of the $Al_3M$ nanophases was sensitive to the temperature, the contribution of formation entropy should not be ignored. The contribution of formation entropy may become very important at high temperature. The entropy change in the alloy consisted of three parts: configuration entropy, hot electron entropy, and vibration entropy. In this calculation, the configuration entropy was generally negligible for a dilute alloy, which was clearly revealed for dilute Al-Sc-Zr alloys [24] and Al-Er-Zr alloys [25], and the hot electron entropy can be ignored for relatively low temperatures [34], so the vibration entropy was considered as contributing to entropy change.

According to the differentiation of Equation (1), the critical nucleation radius of $R$* and the critical nucleation work $\Delta G_V$ *(R*)* can be obtained as:

$$R* = \frac{-2\gamma}{\Delta G_V} \quad (4)$$

$$\Delta G_V(R*) = \frac{16\pi}{3}\frac{\gamma^3}{\Delta G_V^2} \quad (5)$$

The corresponding differences in enthalpy and vibration entropy between the $L1_2$-$Al_3M$ phases and the fcc-$Al_nM$ solution matrix are shown in Table 1. The corresponding differences in enthalpy ($\Delta H_f^{Al_3M} - \Delta H_f^{Al_nM}$) were −0.718 eV/atom, −0.667 eV/atom, −0.823 eV/atom, and −0.902 eV/atom for the $Al_3Sc$ phase, $Al_3Zr$ phase, $Al_3Er$ phase, and $Al_3Y$ phase, respectively. The enthalpy difference of $Al_3Sc$ was in good agreement with the calculated values of −0.72 eV/atom in the literature [33], and was higher than the calculated values of −0.776 eV/atom in the literature [24]. The corresponding enthalpy differences of the $Al_3Zr$ and $Al_3Er$ phases were −0.667 eV/atom and 0.867 ev/atom, respectively, which were also slightly higher than that of the investigation [24,25]. The enthalpy difference of the $Al_3Y$ phase has not yet been documented, but the calculation result was −0.902 eV/atom.

In order to calculate the nucleation work of the $Al_3M$ phase in the Al matrix, it was necessary to calculate the vibration entropy difference. The vibration entropy differences of the $Al_3Sc$ phase, $Al_3Zr$ phase, and $Al_3Er$ phase were 3.35 $k_B$/atom, 4.01 $k_B$/atom, and

5.18 $k_B$/atom, respectively, which were higher than the calculated results in the literature (2.67 $k_B$/Sc [24], 2.72 $k_B$/Zr [24], and3.53 $k_B$/Er [25]). The vibration entropy difference of the $Al_3Y$ phase was 5.72 $k_B$/atom.

**Table 1.** The corresponding enthalpy difference and vibration entropy difference of $L1_2$-$Al_3M$ phase precipitation.

| | $\Delta H_f^{Al_3M} - \Delta H_f^{Al_nM}$ (eV/Atom) | | $\Delta S_{vib}^{Al_3M} - \Delta S_{vib}^{Al_nM}$ ($k_B$/Atom) | |
|---|---|---|---|---|
| $Al_3Sc$-$Al_nSc$ | −0.718 | −0.776 [24] | 3.35 | 2.67 [24] |
| $Al_3Zr$-$Al_nZr$ | −0.667 | −0.831 [24] | 4.01 | 2.72 [24] |
| $Al_3Er$-$Al_nEr$ | −0.823 | −0.867 [25] | 5.18 | 3.53 [25] |
| $Al_3Y$-$Al_nY$ | −0.902 | - | 5.72 | - |

The author's previous research calculated the coherent strain energy of $L1_2$-$Al_3M$/Al [18], where the coherent strain energies were 0.0035 ev/atom for $Al_3Sc$/Al, 0.0023 eV/atom for $Al_3Zr$/Al, 0.0088 eV/atom for $Al_3Er$/Al, and 0.0094 eV/atom for $Al_3Y$/Al. Based on Equations (1)–(3), the computation result at 673 K illustrated that the interface strains contributed to only ~8.5% of the volumetric formation energy for the $Al_3Sc$ phase, the $Al_3Zr$ phase, the $Al_3Er$ phase, and the $Al_3Y$ phase in Al. It indicated that the coherent strain energy of $Al_3M$/Al had little influence on the precipitation of $Al_3M$ nanophases.

Combining with the Al/$Al_3M$ interface energy [18], the critical nucleation radius and critical nucleation work of each phase at 673 K are shown in Table 2. For $L1_2$-$Al_3M$ (M = Sc, Zr, Er, Y), the predicted critical nucleation radii were 5.95 Å, 3.89 Å, 9.57 Å, and 9.40 Å, for the $Al_3Sc$ phase, the $Al_3Zr$ phase, the $Al_3Er$ phase, and the $Al_3Y$ phase, respectively. The critical nucleation works were $2.01 \times 10^{-19}$ J, $4.83 \times 10^{-20}$ J, $6.94 \times 10^{-19}$ J, and $6.84 \times 10^{-19}$ J for the $Al_3Sc$ phase, the $Al_3Zr$ phase, the $Al_3Er$ phase, and the $Al_3Y$ phase, respectively. Among them, the calculated value of the critical nucleation radius of the $Al_3Sc$ phase was slightly lower than the literature value [24], but the critical nucleation radii of the $Al_3Zr$ phase and the $Al_3Er$ phase were slightly higher than the value in Jiang's investigation [24,25]. On the other hand, the critical nucleation work of $Al_3Sc$ was slightly less than the literature value [24], and the critical nucleation works of $Al_3Zr$ and $Al_3Er$ were slightly greater than the literature value [25]. The critical nucleation radius and critical nucleation work of the $Al_3Y$ phase at 673 K has not been reported yet. The investigation of Fan et al. [14] showed that the critical nucleation radius of $Al_3Y$ for the (100) plane was about 3 Å at 300K, which was lower than the calculation value in this research. The reason can be attributed to the different calculation methods of nucleation energy and the low temperature.

**Table 2.** Critical nucleation radius and critical nucleation work.

| | Critical Nucleation Radius (Å) | | Critical Nucleation Work (J) | |
|---|---|---|---|---|
| | Present | Ref. | Present | Ref. |
| $Al_3Sc$ | 5.95 | 6.6 [24] | $2.01 \times 10^{-19}$ | $2.9 \times 10^{-19}$ [24] |
| $Al_3Zr$ | 3.89 | 2.9 [24] | $4.83 \times 10^{-20}$ | $2.9 \times 10^{-20}$ [24] |
| $Al_3Er$ | 9.57 | 8.4 [25] | $6.94 \times 10^{-19}$ | $5.4 \times 10^{-19}$ [25] |
| $Al_3Y$ | 9.40 | - | $6.84 \times 10^{-19}$ | - |

Among the various $L1_2$-$Al_3M$ phases, the $Al_3Zr$ phase obtained the smallest critical nucleation radius and lowest critical nucleation work, whereas the $Al_3Er$ and $Al_3Y$ phases obtained similar nucleation characteristics, and displayed the largest critical nucleation radius and highest critical nucleation work. The critical nucleation radius and nucleation work of $Al_3Sc$ were lower than those of the $Al_3Er$ and $Al_3Y$ phases, which agreed well with Fan's calculation [14]. It indicated that $Al_3Zr$ had thermodynamic advantages in the nucleation process, while the $Al_3Er$ and $Al_3Y$ phases were relatively difficult to nucleate but had advantages in precipitation kinetics.

### *3.2. Nucleation and Stability of Multicomponent $L1_2$-$Al_3M$ Phases*

As described in Section 3.1, the thermodynamic priority order of precipitation was: $Al_3Zr > Al_3Sc > Al_3Er > Al_3Y$. The lowest interface energy of $Al_3Zr/Al$ suggested that the $Al_3Zr$ phase always tended to wrap outside the precipitation phase during the precipitation process. Due to the low interfacial energy of $L1_2$-$Al_3Zr/Al_3Sc$ and $L1_2$-$Al_3Zr/Al_3Er$, once a core–shell structure was formed, the core–shelled $Al_3Sc$ (Zr) and $Al_3Er$ (Zr) were stable structures. However, the previous research showed that $Al_3$(Y, Zr) transformed from a core–shelled structure into a hybrid structure during homogenization at high temperatures [15,16]. In this section, the nucleation of multicomponent $L1_2$-$Al_3$(N, Zr) (N = Y, Sc, Er) phases were investigated based on first-principles thermodynamic calculations. The nucleation of possible ternary $L1_2$-$Al_3$(Y, Zr) phases included the core–shelled structures (the $Al_3$Y-core + $Al_3$Zr-shell structure, denoted as $L1_2$-$Al_3$Zr(Y)), the hybrid structure (denoted as $L1_2$-$Al_3(Zr_x, Y_{1-x})$), and the separate nucleation of binary $L1_2$-$Al_3Zr$ and $L1_2$-$Al_3Y$ (denoted as $L1_2$-$Al_3Zr/Al_3Y$). Moreover, the nucleation calculation result of core–shelled $Al_3$Zr(Y) was also compared with that of core–shelled $Al_3$Zr(Sc,) and core–shelled $Al_3$Zr(Er).

Based on the classical nucleation theory, the structure stability of $L1_2$ nanoparticles with the different structures can be evaluated through the total nucleation energy $\Delta G_{Al_3(N,Zr)}$ (N = Y, Sc, Er), and the expressions are given as [24]:

$$\Delta G_{Al_3Zr(N)} = \frac{4\pi}{3}[(R^3 - r^3)\cdot\Delta G_V^{Al_3Zr} + r^3\cdot\Delta G_V^{Al_3N}] + 4\pi(r^2\cdot\gamma_{Al_3Zr/Al_3N} + R^2\cdot\gamma_{Al_3Zr/Al}) \quad (6)$$

$$\Delta G_{Al_3N+Al_3Zr} = \frac{4\pi}{3}(r^3 \times \Delta G_V^{Al_3N} + r^3 \times \Delta G_V^{Al_3Zr}) + 4\pi(r^2 \times \gamma_{Al/Al_3N} + r^2 \times \gamma_{Al/Al_3Zr}) \quad (7)$$

$$\Delta G_{Al_3(N_x,\ Zr_{1-x})} = \frac{4\pi}{3}R^3\cdot\Delta G_V^{Al_3(N_x,\ Zr_{1-x})} + 4\pi R^2\cdot\gamma_{Al_3(Nx,\ Zr1-x)} \quad (8)$$

Here *R* is the radius of ternary $L1_2$-$Al_3$(N, Zr), and *r* is the radius of the binary $Al_3N$. Assuming that all the solute atoms had completely precipitated from the Al matrix, the *R* and *r* values of ternary $L1_2$-$Al_3$(N, Zr) with a core–shelled structure depended on the relative precipitation amount of solute atoms N and Zr. $\Delta G_V^{Al_3N}$ and $\Delta G_V^{Al_3Zr}$ are the volumetric formation energy of the $L1_2$-$Al_3N$ phase and the $Al_3Zr$ phase in aluminum alloys. $\gamma_{Al_3Zr/Al_3N}$ and $\gamma_{Al_3Zr/Al}$ are the interface energies of the $Al_3Zr/Al_3N$ and $Al_3Zr/Al$ interface in aluminum alloys. The $Al_3Zr(001)/Al_3N(001)$-contacting facets were considered to be the most energy-favored orientation, and the interfaces' energies were calculated in the authors' previous investigation [18]. It should be noted that the interfaces' energies were generally oerestimated at the actual precipitation temperature due to the density functional principles of the ground state. $\Delta G_V^{Al_3(N_x,\ Zr_{1-x})}$ and $\gamma_{Al_3(N_x,\ Zr_{1-x})}$ are the volumetric formation energy and the interface energy of the hybrid structure of $Al_3(N_x, Zr_{1-x})$. However, it was difficult to directly calculate the value of $\Delta G_V^{Al_3(N_x,\ Zr_{1-x})}$, which was estimated by the composition-weighted summation of $\Delta G_V^{Al_3N}$ and $\Delta G_V^{Al_3Zr}$ [24]. Similarly, $\gamma_{Al_3(N_x,\ Zr_{1-x})}$ was evaluated by the composition-weighted summation of $\gamma_{Al_3N/Al}$ and $\gamma_{Al_3Zr/Al}$.

Furthermore, the authors' previous investigation indicated that Er atoms tended to segregate at the $Al_3Y/Al_3Zr$ interface, and were inclined to form a core–double-shelled $Al_3Y/Al_3Er/Al_3Zr$ structure [18], denoted as $Al_3$Zr/Er(Y), and its nucleation energy and thermodynamic stability can be evaluated as:

$$\begin{aligned}\Delta G_{Al_3Zr/Er(Y)} = {} & \tfrac{4\pi}{3}[(R_2^3 - R_1^3) \times \Delta G_V^{Al_3Zr} + (R_1^3 - r^3) \times \Delta G_V^{Al_3Er} + r^3 \times \Delta G_V^{Al_3Y}) \\ & +4\pi(r^2 \times \gamma_{Al_3Y/Al_3Er} + R_1^2 \times \gamma_{Al_3Zr/Al_3Er} + R_2^2 \times \gamma_{Al_3Zr/Al})\end{aligned} \quad (9)$$

Here $R_1$ and $R_2$ are the radii of the first and second shells of the core–double-shelled $Al_3Zr/Er$ (Y), respectively; $r$ is the radius of the $Al_3Y$ core layer.

Under the conditions of homogenization temperature (T = 673 K) and the equal solute atomic ratio (the atomic ratio of Y to Zr was 1), the total nucleation energies ($\Delta G$) of the various possible structures for the $L1_2$-$Al_3$(Y, Zr) phase were calculated as a function of the precipitate radius (R), and the results are plotted in Figure 1. It showed that the nucleation energy of various structures of $Al_3$(Y, Zr) increased with the radius of the precipitated phase. At a radius of 0–1 nanometers, there was no significant difference in the free energy of each phase; thus, several structures of $Al_3$(Y, Zr) phases can coexist in the early stage of homogenization. To some extent, the 0–1 nanometer precipitation stage corresponded to the early aging stage of atomic clusters, and did not form a stable microstructure.

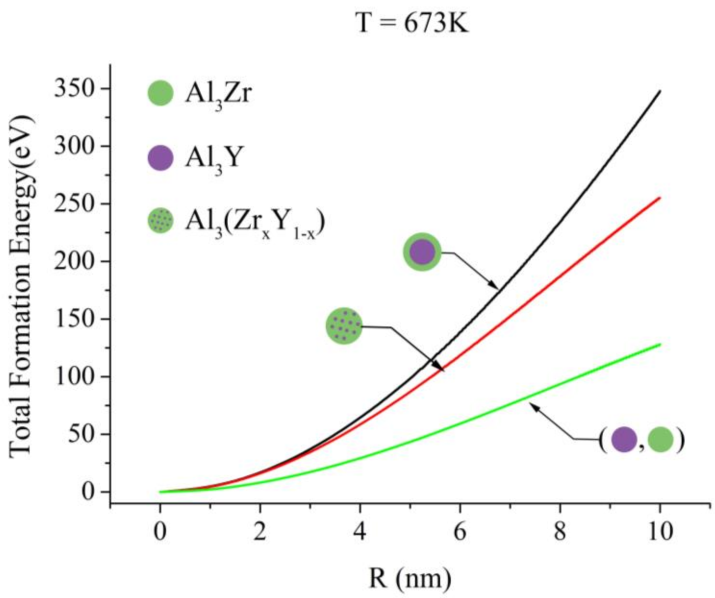


**Figure 1.** Relationship between nuclear energy and the radii of various structures of $Al_3$(Y, Zr) at the homogenization temperature of 673 K and the equal stoichiometric ratio.

At a radius of 1–10 nanometers, the difference in the total nucleation energy among different structures became increasingly significant. The core–shelled $Al_3Zr$(Y) phase illustrated the highest nucleation work among various precipitate structures, indicating that the core–shelled $Al_3Zr$(Y) phase precipitated without advantage in thermodynamics. However, the separated nucleation of binary $L1_2$-$Al_3Zr/Al_3Y$ obtained the lowest nucleation energy, suggesting that $L1_2$-$Al_3Zr/Al_3Y$ had thermodynamic advantages in the nucleation process. Due to the low segregation energy of Zr elements at the $Al_3Y$ interface, it was beneficial to drive the segregation of Zr elements at the $Al_3Y$ interface [18]. Gao et al. [16] studied the early precipitation phase structure of Al-0.08Y-0.30Zr alloy at 350 °C for 10 min, and the results showed that the precipitation phase was mainly the $Al_3Y$ phase, which became the core of $Al_3Zr$ and promoted the precipitation kinetics of solid solution Zr atoms. However, it was difficult to form a stable core–shelled $Al_3Y/Al_3Zr$ owing to the large coherency strain energy and high mismatch between $Al_3Y$ and $Al_3Zr$ [18]. Thus, the separated structure of $L1_2$-$Al_3Zr/Al_3Y$ was considered to be the thermodynamically stable structure. The investigation by Gao et al. [16] showed that after isothermal aging at 400 °C for 200 h, the Y and Zr atoms in the Al-Y-Zr alloy were almost uniformly distributed within the precipitate phase, indicating a separated structure of $L1_2$-$Al_3Zr/Al_3Y$, and did not exhibit a clear core–shelled structure, which confirmed the first-principles calculation results in this paper.

Figure 2 shows the total nucleation energies ($\Delta G$) for three kinds of core–shelled structures, $Al_3Zr$(Sc), $Al_3Zr$(Er), and $Al_3Zr$(Y), under the condition of homogenization at

673 K and the complete precipitation of Sc, Y, Er, and Zr in equal proportion, respectively. The nucleation energies of core–shelled $Al_3Zr(Y)$ and $Al_3Zr(Sc)$ increased with the radius of the precipitated phase, whereas the nucleation energies of $Al_3Zr(Er)$ were negative, and decreased with the radius of the precipitated phase. The calculations of $Al_3Zr(Sc)$ and $Al_3Zr(Er)$ were similar to the investigation by Jiang et al. [24,25]. The order of the nucleation energies was: $Al_3Zr(Y) > Al_3Zr(Sc) > Al_3Zr(Er)$. The core–shelled $Al_3Zr(Y)$ phase obtained the highest nucleation energy, indicating that it was inclined to form a separated structure, $L1_2$-$Al_3Zr/Al_3Y$, which was very consistent with the experimental observation [16]. The core–shelled $Al_3Zr(Sc)$ and $Al_3Zr(Er)$ were thermodynamically stable structures owing to their low nucleation energies, which were confirmed by the experimental observation in Al-Sc-Zr alloys [8] and Al-Er-Zr alloys [9]. In comparison with $Al_3Zr(Y)$ and $Al_3Zr(Sc)$, although the $Al_3Er/Al_3Zr$ interface had a higher coherent strain energy than that the of $Al_3Sc/Al_3Zr$ interface [18], core-shelled $Al_3Zr(Er)$ obtained a low nucleation energy due to its low chemical energy $\Delta G_{chem}$ and the $Al_3Er/Al_3Zr$ interface energy. Thus, the nucleation energy of $Al_3M$ nanophases depended on their chemical energy $\Delta G_{chem}$ and the interface energy.

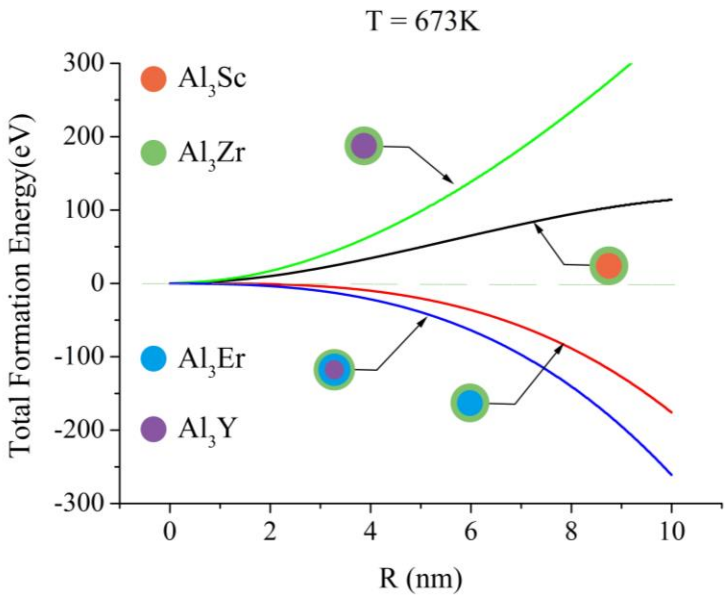


**Figure 2.** Relationship between nuclear energy and the radii of various structures of $L1_2$-$Al_3(N, Zr)$ (N = Er, Y, Sc) at the homogenization temperature of 673 K and the equal stoichiometric ratio.

The nucleation energies ($\Delta G$) of core–double-shelled $Al_3Zr/Er(Y)$ were carried out under the condition of homogenization at 673 K and the complete precipitation of Y, Er, and Zr in equal proportion. The nucleation energy of $Al_3Zr/Er(Y)$ was negative and significantly decreased with the precipitation radius, as shown in Figure 2. The nucleation energy of $Al_3Zr/Er(Y)$ was far lower than that of core–shelled $Al_3Zr(Y)$, and obtained high thermodynamic stability, preferentially precipitating in thermodynamics. Core–double-shelled $Al_3Zr/Er(Y)$ was inclined to form in Al-Y-Er--Zr alloys, as the Er atom tended to segregate at the $Al_3Y/Al_3Zr$ interface [18]. The segregation of the Er atom dramatically decreased the nucleation energy due to the decrease in $\Delta G_{chem}$ and strain energy $G_S$, as illustrated in $Al_3Zr(Er)$, although the high interfacial energy of $Al_3Y/Al_3Er$ replaced the relatively low interface energy of $Al_3Y/Al_3Zr$. Interestingly, the nucleation energy of $Al_3Zr/Er(Y)$ was even lower than that of $Al_3Zr(Er)$ due to the addition of the Y atom, which can be attributed to the negative interface energy of $Al_3Er/Al_3Y$ and low coherent strain energy $G_s$. Similarly, in the Al-Sc-Zr aluminum alloy, the addition of the Er atom formed a core–double-shelled $Al_3Zr/Sc$ (Er) instead of forming separated $Al_3$(Sc, Zr) and $Al_3$(Er, Zr) [20], which was attributed to the decreased nucleation energy of $Al_3$(Sc, Zr) nanoparticles by its low chemical energy $\Delta G_{chem}$. Therefore, the design of the core–double-shelled $Al_3Zr/Er(Y)$ nanophase can provide guidance for the development of new Al-Er-Y-Zr alloys.

## 4. Conclusions

Based on the first-principles thermodynamic calculation, the nucleation energies of the $L1_2$-$Al_3M$ (M = Sc, Zr, Er, Y) nanophases in aluminum alloys were studied combined with classical nucleation theory. The conclusions were as follows:

(1) The critical radius and nucleation work of the $L1_2$-$Al_3M$ precipitate phase were as follows: $Al_3Er > Al_3Y > Al_3Sc > Al_3Zr$. The $Al_3Zr$ phase was the easiest to nucleate in thermodynamics, while the nucleation of the $Al_3Y$ and $Al_3Er$ phases were relatively difficult in thermodynamics.

(2) Various structures of $Al_3(Y, Zr)$ phases with the radius r < 1 nm can coexist in Al-Y-Zr alloys. At a precipitate's radius of 1–10 nanometers, the core–shelled $Al_3Zr(Y)$ phase illustrated the highest nucleation energy, while the separated structure, $Al_3Zr/Al_3Y$, obtained the lowest one, and had thermodynamic advantages in the nucleation process.

(3) Core–double-shelled $Al_3Zr/Er(Y)$ obtained a lower nucleation energy than that of $Al_3Zr(Y)$ due to the negative $\Delta G_{chem}$ of $Al_3Er$ and the negative $Al_3Er/Al_3Y$ interface energy, and preferentially precipitated in thermodynamics stability.

**Author Contributions:** B.N. and Y.S. conceived and designed the research; S.L., F.L. and Z.Y. performed the first-principles calculation; T.F. and D.C. analyzed the experimental data; S.L. wrote the manuscript. All authors have read and agreed to the published version of the manuscript.

**Funding:** This research was funded by the R & D plan for key areas in Guangdong Province (2020B01 0186001), the Science and Technology Program of the Ministry of Science and Technology (G2022030060L), the Science and technology project in Guangdong (2020b15120093, 2020B121202002), the Science and technology research project of Foshan (1920001000412, 2220001005305), and the R and D plan for key areas in Jiangxi Province (20201BBE51009, 20212BBE51012).

**Data Availability Statement:** The data presented in this study are available on request from the corresponding author.

**Conflicts of Interest:** The authors declare no conflict of interest.

## References

1. Liu, L.; Xu, G.; Deng, Y.; Yu, Q.; Li, G.; Zhang, L.; Liu, B.; Fu, L.; Pan, Q. Existing form of Sc in metal-inert gas welded Al-0.60 Mg-0.75 Si alloy and its role in welding strength. *Mater. Charact.* **2023**, *197*, 112649. [CrossRef]
2. Ye, J.; Pan, Q.; Liu, B.; Hu, Q.; Qu, L.; Wang, W.; Wang, X. Effects of co-addition of minor Sc and Zr on aging precipitates and mechanical properties of Al-Zn-Mg-Cu alloys. *J. Mater. Res. Technol.* **2023**, *22*, 2944–2954. [CrossRef]
3. Deng, P.; Mo, W.; Ouyang, Z.; Tang, C.; Luo, B.; Bai, Z. Mechanical properties and corrosion behaviors of (Sc, Zr) modified Al-Cu-Mg alloy. *Mater. Charact.* **2022**, *196*, 112619. [CrossRef]
4. Zha, M.; Tian, T.; Jia, H.L.; Zhang, H.M.; Wang, H.Y. Sc/Zr ratio-dependent mechanisms of strength evolution and microstructural thermal stability of multi-scale hetero-structured Al–Mg–Sc–Zr alloys. *J. Mater. Sci. Technol.* **2023**, *140*, 67–78. [CrossRef]
5. De Luca, A.; Seidman, D.N.; Dunand, D.C. Effects of Mo and Mn microadditions on strengthening and over-homogenization resistance of nanoprecipitation-strengthened Al-Zr-Sc-Er-Si alloys. *Acta Mater.* **2019**, *165*, 1–14. [CrossRef]
6. Booth-Morrison, C.; Mao, Z.; Diaz, M.; Dunand, D.C.; Wolverton, C.; Seidman, D.N. Role of silicon in accelerating the nucleation of $Al_3(Sc, Zr)$ precipitates in dilute Al-Sc-Zr alloys. *Acta Mater.* **2012**, *60*, 4740–4752. [CrossRef]
7. Senkov, O.N.; Shagiev, M.R.; Senkova, S.V.; Miracle, D.B. Precipitation of $Al_3(Sc, Zr)$ particles in an Al-Zn-Mg-Cu-Sc-Zr alloy during conventional solution heat treatment and its effect on tensile properties. *Acta Mater.* **2008**, *56*, 3723–3738. [CrossRef]
8. Forbord, B.; Lefebvre, W.; Danoix, F.; Hallem, H.; Marthinsen, K. Three dimensional atom probe investigation on the formation of $Al_3(Sc, Zr)$-dispersoids in aluminium alloys. *Scripta Mater.* **2004**, *51*, 333–337. [CrossRef]
9. Wu, H.; Wen, S.P.; Huang, H.; Li, B.L.; Wu, X.L.; Gao, K.Y.; Wang, W.; Nie, Z.R. Effects of homogenization on precipitation of $Al_3(Er, Zr)$ particles and recrystallization behavior in a new type Al-Zn-Mg-Er-Zr alloy. *Mater. Sci. Eng. A* **2017**, *689*, 313–322. [CrossRef]
10. Leibner, M.; Vlach, M.; Kodetová, V.; Kudrnová, H.; Veselý, J.; Zikmund, S.; Čížek, J.; Melikhova, O.; Lukáč, F. Effect of deformation on evolution of $Al_3(Er, Zr)$ precipitates in Al-Er-Zr-based alloy. *Mater. Charact.* **2022**, *186*, 111781. [CrossRef]

11. Peng, G.; Chen, K.; Fang, H.; Chen, S. A study of nanoscale $Al_3$(Zr, Yb) dispersoids structure and thermal stability in Al–Zr–Yb alloy. *Mater. Sci. Eng. A* **2012**, *535*, 311–315. [CrossRef]
12. Pang, H.C.; Shang, P.J.; Huang, L.P.; Chen, K.H.; Liu, G.; Xiong, X. Precipitates and precipitation behavior in Al–Zr–Yb–Cr alloys. *Mater. Lett.* **2012**, *75*, 192–195.
13. Hu, T.; Ruan, Z.; Fan, T.; Wang, K.; He, K.; Wu, Y. First-principles investigation of the diffusion of TM and the nucleation and growth of $L1_2$ $Al_3$TM particles in Al alloys. *Crystals* **2023**, *13*, 1032. [CrossRef]
14. Fan, T.; Ruan, Z.; Zhong, F.; Xie, C.; Li, X.; Chen, D.; Tang, P.; Wu, Y. Nucleation and growth of $L1_2$-$Al_3$RE particles in aluminum alloys: A first-principles study. *J. Rare Earths* **2023**, *41*, 1116–1126. [CrossRef]
15. Zhang, Y.; Gu, J.; Tian, Y.; Gao, H.; Wang, J.; Sun, B. Microstructure evolution and mechanical property of Al–Zr and Al–Zr–Y alloys. *Mater. Sci. Eng. A* **2014**, *616*, 132–140. [CrossRef]
16. Gao, H.; Feng, W.; Wang, Y.; Gu, J.; Zhang, Y.; Wang, J.; Sun, B. structure and compositional evolution of $Al_3$(Zr, Y) precipitates in Al-Zr-Y alloy. *Mater. Charact.* **2016**, *121*, 195–198. [CrossRef]
17. Wang, Y.; Miao, Y.; Peng, P.; Gao, H.; Wang, J.; Sun, B. Ab initio investigation on preferred orientation at the Al/$Al_3$(Zr, Y) interface in Al–Zr–Y alloy. *J. Appl. Phys.* **2022**, *131*, 225111. [CrossRef]
18. Song, Y.; Zhan, S.; Nie, B.; Liu, S.; Qi, H.; Liu, F.; Fan, T.; Chen, D. First-principle investigation of the interface properties of the core-shelled $L1_2$-$Al_3$M (M = Sc, Zr, Er, Y) phase. *Crystals* **2023**, *13*, 420. [CrossRef]
19. Dorin, T.; Babaniaris, S.; Jiang, L.; Cassel, A.; Eggeman, A.; Robson, J. Precipitation sequence in Al-Sc-Zr alloys revisited. *Materialia* **2022**, *26*, 101608. [CrossRef]
20. Booth-Morrison, C.; Dunand, D.C.; Seidman, D.N. Coarsening resistance at 400 °C of precipitation-strengthened Al–Zr–Sc–Er alloys. *Acta Mater.* **2011**, *59*, 7029–7042. [CrossRef]
21. Leibner, M.; Vlach, M.; Kodetová, V.; Veselý, J.; Čížek, J.; Kudrnová, H.; Lukáč, F. On the Sc-rich core of $Al_3$(Sc, Er, Zr) precipitates. *Mater. Lett.* **2022**, *325*, 132759. [CrossRef]
22. Qian, W.; Zhao, Y.; Kai, X.; Gao, X.; Huang, L.; Miao, C. Characteristics of microstructureand mechanical evolution in 6111Al alloy containing $Al_3$(Er, Zr) nanoprecipitates. *Mater. Charact.* **2021**, *178*, 111310. [CrossRef]
23. Zhang, J.; Hu, T.; Yi, D.; Wang, H.; Wang, B. Double-shell structure of $Al_3$(Zr, Sc) precipitate induced by thermomechanical treatment of Al–Zr–Sc alloy cable. *J. Rare Earths* **2019**, *37*, 668–672. [CrossRef]
24. Zhang, C.; Jiang, Y.; Cao, F.; Hu, T.; Wang, Y.; Yin, D. Formation of coherent, core-shelled nano-particles in dilute Al-Sc-Zr alloys from the first-principles. *J. Mater. Sci. Technol.* **2019**, *35*, 930–938. [CrossRef]
25. Zhang, C.; Yin, D.; Jiang, Y.; Wang, Y. Precipitation of $L1_2$-phase nano-particles in dilute Al-Er-Zr alloys from the first-principles. *Comp. Mater. Sci.* **2019**, *162*, 171–177. [CrossRef]
26. Liu, X.; Wang, Q.; Zhao, C.; Li, H.; Wang, M.; Chen, D.; Wang, H. Formation of ordered precipitates in Al-Sc-Er-(Si/Zr) alloy from first-principles study. *J. Rare Earths* **2023**, *9*, 609–620. [CrossRef]
27. Nityananda, R.; Hohenberg, P.; Kohn, W. Inhomogeneous electron gas. *Resonance* **2017**, *22*, 809–811. [CrossRef]
28. Kresse, G.; Furthmüller, J. Efficiency of ab-initio total energy calculations for metals and semiconductors using a plane-wave basisset. *Comp. Mater. Sci.* **1996**, *6*, 15–50. [CrossRef]
29. Kresse, G.; Joubert, D. From ultrasoft pseudopotentials to the projector augmented-wave method. *Phys. Rev. B* **1999**, *59*, 1758–1775. [CrossRef]
30. Perdew, J.P.; Burke, K.; Ernzerhof, M. Generalized Gradient Approximation Made Simple. *Phys. Rev. Lett.* **1998**, *77*, 3865–3868. [CrossRef]
31. Budimir, M.; Damjanovic, D.; Setter, N. Piezoelectric Response and Free Energy Instability in the Perovskite Crystals $BaTiO_3$, $PbTiO_3$ and Pb(Zr, Ti)$O_3$. *Phys. Rev. B* **2006**, *73*, 4106. [CrossRef]
32. Baroni, S.; De Gironcoli, S.; Dal Corso, A.; Giannozzi, P. Phonons and related crystal properties from density-functional perturbation theory. *Rev. Mod. Phys.* **2001**, *73*, 515. [CrossRef]
33. Mao, Z.; Chen, W.; Seidman, D.N.; Wolverton, C. First-principles study of the nucleation and stability of ordered precipitates in ternary Al–Sc–Li alloys. *Acta Mater.* **2011**, *59*, 3012–3023. [CrossRef]
34. Swan-Wood, T.L.; Delaire, O.; Fultz, B. Vibrational entropy of spinodal decomposition in FeCr. *Phys. Rev. B* **2005**, *72*, 024305. [CrossRef]